

FSU-HEP-950204  
UH-511-817-95

# SIGNALS FOR MINIMAL SUPERGRAVITY AT THE CERN LARGE HADRON COLLIDER: MULTI-JET PLUS MISSING ENERGY CHANNEL

Howard Baer<sup>1</sup>, Chih-hao Chen<sup>1</sup>, Frank Paige<sup>2</sup>  
and Xerxes Tata<sup>3</sup>

<sup>1</sup>*Department of Physics, Florida State University, Tallahassee, FL 32306 USA*

<sup>2</sup>*Brookhaven National Laboratory, Upton, NY 11973 USA*

<sup>3</sup>*Department of Physics and Astronomy, University of Hawaii, Honolulu, HI 96822 USA*  
(September 17, 2018)

## Abstract

We use ISAJET to perform a detailed study of the missing transverse energy  $\cancel{E}_T$  plus multi-jet signal expected from superparticle production at the CERN LHC. Our analysis is performed within the framework of the minimal supergravity model with gauge coupling unification and radiative electroweak symmetry breaking. We delineate the region of parameter space where the  $\cancel{E}_T$  supersymmetry signal should be observable at the LHC and compare it to the regions explorable via searches for sleptons and for chargino/neutralino production. We confirm that, given a data sample of  $10 \text{ fb}^{-1}$ ,  $m_{\tilde{g}} \sim 1300 \text{ GeV}$  can be explored if  $m_{\tilde{q}} \gg m_{\tilde{g}}$ , while  $m_{\tilde{g}} \sim 2000 \text{ GeV}$  can be probed if  $m_{\tilde{q}} \simeq m_{\tilde{g}}$ . We further examine what information can be gleaned from scrutinizing this event sample. For instance, the multi-jet multiplicity yields information on whether squark production makes a significant contribution to the observed  $\cancel{E}_T$  sample. Furthermore, reconstructing hemispheric masses may yield a measure of  $m_{\tilde{g}}$  to  $\sim 15 - 25\%$ . Finally, for favourable ranges of parameters, by reconstructing masses of tagged  $b\bar{b}$  jet pairs, it may be possible to detect Higgs bosons produced via sparticle cascade decay chains.

## I. INTRODUCTION

### A. Motivation and Framework

The existence of weak-scale supersymmetry (SUSY), stabilizing the electroweak symmetry breaking sector of the Standard Model (SM), is a tantalizing hypothesis [1]. This hypothesis has received some support from the observation that the running gauge couplings unify at a scale  $M_X \sim 10^{16}$  GeV provided that the superpartners have masses  $\sim 1$  TeV, while this unification does not occur in the SM [2]. Hence, the search for supersymmetric particles is a high priority task for collider experiments. Expectations for super-particle masses are typically in the 100–1000 GeV range, whereas current limits on them are generally below  $M_Z/2$  [3], although the CDF and D0 experiments at the Tevatron probe gluinos and squarks as heavy as 150–200 GeV [4]. In the near future, LEP II will probe slepton and chargino masses up to  $m_{\tilde{l}}, m_{\tilde{W}_1} \sim 90$  GeV, while Tevatron experiments, for favourable parameter ranges, may indirectly reach  $m_{\tilde{g}} \sim 500$  GeV in the main injector era, via the clean tri-lepton signal from  $\tilde{W}_1 \tilde{Z}_2$  production [5–7]. These experiments have a good chance to discover weak scale supersymmetry, but they cannot exclude it. A thorough search for low-energy supersymmetry can only be made at the recently approved CERN Large Hadron Collider (LHC) or, alternatively, at  $e^+e^-$  linear colliders with center of mass energies exceeding 500–1000 GeV [8,7].

Most early analyses were carried out within the framework of the Minimal Supersymmetric Model (MSSM), which is the supersymmetric extension of the SM with the least number of additional new particles and interactions necessary for phenomenology. As a consequence,  $R$ -parity is exactly conserved, so that the lightest SUSY particle (LSP) is stable. Supersymmetry breaking is parametrized by the introduction of soft SUSY breaking mass terms and interactions consistent with the SM gauge group. Since each  $SU(3) \times SU(2) \times U(1)$  multiplet of sfermions and gauginos has an independent mass, the most general parametrization of SUSY breaking requires a large number of mass parameters, and also many arbitrary trilinear scalar couplings.

Without further assumptions about these parameters, any phenomenological analysis is essentially intractable. Motivated by grand unified theories (GUTs), we shall, following the early SUSY analyses in Ref. [9–11], further assume that the three  $\overline{DR}$  gaugino masses originate in a common gaugino mass at some high scale, so that the ratios of these masses at the weak scale are proportional to the corresponding ratios of the squared gauge couplings. The  $SU(2)$  and  $U(1)$  gaugino masses are then determined in terms of  $m_{\tilde{g}}$ . Motivated by supergravity models, these analyses further assumed a common *physical* mass for each of the light squarks, left and right sleptons, and sneutrinos. The Higgs sector of this model is determined at tree level by  $m_{H_p}$ , the mass of the neutral pseudoscalar, in addition to the parameters  $\tan \beta$ , the ratio of the two vacuum expectation values, and  $\mu$ , the superpotential Higgsino mass (which also enter the gaugino-Higgsino sector). Finally, the weak-scale  $A$ -parameters, which mainly affect the phenomenology of third generation squarks were needed to completely specify the model. In what follows, and in the simulation program ISAJET [12], we use the term MSSM to refer to this supergravity-inspired framework.

In view of the fact that the additional assumptions for the MSSM are motivated by supergravity GUT models, it seems reasonable to seriously explore their implications. The

assumptions underlying these models, which differ in important ways from those of the MSSM, are outlined below. Several phenomenological analyses of supergravity models [13] have recently appeared in the literature [14,16,15,17]. In minimal supergravity with canonical kinetic energy terms, gravitational interactions communicate the effects of supersymmetry breaking in a hidden sector to the observable sector of particles. These gravitational interactions, being universal, lead to a common mass ( $m_0$ ) for all scalar fields and common trilinear and bilinear soft SUSY breaking ( $A_0$  and  $B_0$ ) scalar interactions [18]. The resulting Lagrangian should be regarded as an effective Lagrangian of the theory below the Planck scale, with its parameters renormalized at some ultra-high energy scale close to  $M_{Planck}$ . If we further assume that these interactions respect an (unbroken) GUT symmetry, the gauginos must all be part of a single multiplet, and so must have a common mass ( $m_{1/2}$ ) at this scale. Similar considerations also apply to string models, which can lead to coupling constant unification without a grand unifying gauge group [19]. The SUSY breaking sector of the model is then completely specified by these four parameters.

For phenomenological analyses, the running parameters in the Lagrangian should be renormalized at the weak scale to sum the large logarithms arising from the disparity between the high scale where the physics is simple, and the weak scale relevant to collider phenomenology. This is most conveniently done using renormalization group (RG) equations [20] and taking the common values of the four high-scale input parameters as boundary conditions. The RG evolution splits the various masses and leads to a rich spectrum at the weak scale [21]. The first two generations of squarks are approximately degenerate, so these models automatically satisfy constraints [22] from the non-observation of flavour changing neutral currents in the kaon sector, while  $\tilde{t}_1$ , the lighter  $t$ -squark and  $\tilde{b}_1 \sim \tilde{b}_L$ , the lighter  $b$ -squark, may be substantially lighter. Sleptons are lighter than squarks, and may be much lighter if gluinos and squarks of the first two generations have comparable masses. As a bonus, the RG evolution also gives the correct pattern of electroweak symmetry breaking [23,20] for considerable ranges of input parameters. It is customary to eliminate  $B_0$  in favour of  $\tan \beta$  and to adjust the value of  $\mu$  to reproduce the measured  $Z$  boson mass. Then the particle/sparticle masses and couplings are determined by the following parameters (along with  $m_t$ ):

$$m_0, m_{1/2}, A_0, \tan \beta, \text{ and } \text{sgn}(\mu). \quad (1)$$

In particular, the values of the MSSM parameters  $\mu$  and  $m_{H_p}$  are determined. Typically,  $\mu$  is large, so that the lighter charginos and neutralinos are dominantly gaugino-like, while the heavier ones are dominantly Higgsino-like. Also,  $m_{H_p} \gg M_W$  so the lightest Higgs scalar ( $H_\ell$ ) resembles a SM Higgs boson with the other Higgs particles all relatively heavy. In what follows, we shall use the term SUGRA to mean supersymmetry with masses and mixings calculated from the parameters in equation (1).

The simulation program ISAJET [12] now allows the user either to specify the weak-scale MSSM parameters — the gluino, squark, stop, sbottom and slepton masses,  $A$ -parameters,  $\mu$ ,  $m_{H_p}$  and  $\tan \beta$  — or to use values of these parameters calculated from the SUGRA parameter set (1). Because the SUGRA model is specified by just four new parameters, various experimental observables that can be determined in experiments at colliders become correlated and so provide non-trivial tests of the underlying assumptions [14,17,7]. It is, however, worth remembering that SUGRA models are based on extrapolations of physics which may

ultimately prove incorrect. While these models are indeed very attractive, economical, and satisfy all phenomenological constraints, it may be worthwhile to test the sensitivity of model predictions by running ISAJET using the optional MSSM input set, which is a more general framework that can encompass models with non-universal soft-breaking sfermion mass terms. This may be particularly important for assessing the reach of future facilities.

## B. Phenomenological Overview

Since strongly interacting sparticles are most copiously produced at hadron colliders, many of the early studies of supersymmetry at hadron supercolliders focussed on the detection of gluinos and squarks [9–11]. Recently, a number of papers addressing the detection of weakly interacting sparticles at the LHC have also appeared. In Ref. [24], it was shown that LHC experiments ought to be able to detect clean dileptons from slepton pair production if  $m_{\tilde{l}} \lesssim 200\text{--}250$  GeV. Also, in Ref. [25], it was shown that LHC experiments ought to be able to detect the clean trilepton signal from  $\tilde{W}_1 \tilde{Z}_2$  production over much of parameter space as long as the two body decays  $\tilde{Z}_2 \rightarrow H_\ell \tilde{Z}_1$  and  $\tilde{Z}_2 \rightarrow Z \tilde{Z}_1$  are kinematically inaccessible. Experiments at a high luminosity upgrade of the Tevatron may have a similar reach as the LHC if  $\mu$  is negative; for positive values of  $\mu$  the branching fraction for the three body decays  $\tilde{Z}_2 \rightarrow \ell \bar{\ell} \tilde{Z}_1$  is strongly suppressed, and the corresponding reach at the Tevatron is somewhat smaller than at the LHC.

Direct slepton pair and chargino/neutralino production takes place via weak interactions, whereas the strength of the LHC lies in the production of strongly interacting particles. In Fig. 1, we show the total production cross sections at  $\sqrt{s} = 14$  TeV for strongly interacting SUSY particles ( $\tilde{g}\tilde{g}$ ,  $\tilde{g}\tilde{q}$  and  $\tilde{q}\tilde{q}$ ), for charginos and neutralinos in association with squarks and gluinos, and for gaugino pairs ( $\tilde{W}_1 \tilde{Z}_2$  and  $\tilde{W}_1 \tilde{W}_1$ ), as a function of  $m_{\tilde{g}}$ . We have assumed gaugino mass unification and 5 degenerate species of L- and R-squarks, taken  $\mu = -m_{\tilde{g}}$  and  $\tan \beta = 2$ , and used the CTEQ2L parton distribution functions [26]. In Fig. 1a, we take  $m_{\tilde{q}} = m_{\tilde{g}}$ , while in Fig. 1b we take  $m_{\tilde{q}} = 2m_{\tilde{g}}$ . In a), it is clear that strong sparticle production is the dominant production mechanism at the LHC for all values of  $m_{\tilde{g}}$  from 300 GeV out to 2000 GeV. In b), strong sparticle pair production is dominant up to  $m_{\tilde{g}} \sim 1100$  GeV, after which chargino/neutralino production becomes dominant. In both cases, associated production mechanisms are sub-dominant cross sections, even though the combined mass of the produced sparticles can be much smaller than the mass of a pair of strongly interacting sparticles. The fact that strongly-produced sparticle pairs are the dominant production mechanism for squarks and gluinos as heavy as 1–2 TeV leads us to focus on signals from squarks and gluinos.

Once gluinos and squarks are produced, they are expected to decay through various channels until the cascade terminates in the stable LSP (taken to be  $\tilde{Z}_1$ ) [27]. These cascade decays lead to final states containing multiple jets, isolated and non-isolated leptons, and missing transverse energy (mainly from the undetected  $\tilde{Z}_1$ 's and neutrinos). Rates for the various multi-lepton signatures have been presented in Ref. [28]; the most promising signatures appeared to be those containing same-sign isolated dileptons [29], and isolated trileptons. The multi-jet +  $E_T$  signal, while generally much larger than signals from multi-leptons, is less clean, due to irremovable backgrounds from various SM QCD induced

processes (multi-jet production, vector boson production in association with jets and heavy flavor production).

Detailed studies of the missing energy plus multi-jet signal have been performed by the GEM [11] and SDC [10] collaborations for the now defunct Superconducting Supercollider project [30]. More recently, detailed studies of this same signature have also been performed by the ATLAS [31] Collaboration for the CERN LHC. In these LHC studies, performed within the framework of the supergravity-inspired MSSM, it was shown that values of  $m_{\tilde{g}} \sim 1300$  GeV ( $m_{\tilde{g}} \sim 2000$  GeV) could be probed for  $m_{\tilde{q}} \gg m_{\tilde{g}}$  ( $m_{\tilde{q}} \sim m_{\tilde{g}}$ ), given  $10 \text{ fb}^{-1}$  of integrated luminosity. In addition, values of  $m_{\tilde{g}}$  as low as 300 GeV could easily be probed at the LHC, so that there should be no “gap” in the explorable range of  $m_{\tilde{g}}$  between Tevatron searches and future LHC searches.

In the present paper, we further scrutinize the missing energy plus multi-jet signal. Our goals are multiple:

1. We update previous results [28] on multijet  $+ \cancel{E}_T$  cross sections by using the latest ISAJET 7.13 simulation for sparticle production and cascade decays.
2. We evaluate the reach of the LHC via some set of optimized cuts, valid across a large range of sparticle mass choices.
3. We present our reach results in the parameter space of the minimal supergravity model with gauge coupling unification and radiative electroweak symmetry breaking. The rather small parameter set yields a correlated spectrum of SUSY particle masses, and allows one to compare the regions of parameter space that different search experiments can probe.
4. We examine what information can be gleaned from a sample of signal events in the missing energy plus multi-jet channel. For instance, can one tell whether the signal is mainly due to gluino production, or whether  $\tilde{q}\tilde{q}$  and  $\tilde{g}\tilde{g}$  production is also significant? Can one gain some sort of mass measurement for the gluino or squark? Can one identify the presence of other particles or sparticles by sifting through the debris of the cascade decay?

The first three of these points are addressed in Sec. II of this paper, where we mainly map out regions of SUGRA parameter space explorable by LHC experiments using the multi-jet plus missing energy signature. We also compare these regions with those where various slepton and chargino/neutralino searches are expected to result in observable signals. In Sec. III, we address the questions raised above in item (4), and find that to some degree, and at least in some cases, all the questions raised can be answered in the affirmative. We summarize our results and present our conclusions in Sec. IV.

## II. REACH OF THE LHC IN SUGRA PARAMETER SPACE

### A. Event simulation

In this paper, we work within the framework of the minimal SUGRA model, as implemented in the ISAJET 7.13 subprogram ISASUGRA [17]. The SUGRA parameter set (1)

can be directly entered into ISAJET, and ISASUGRA then calculates all the SUSY particle masses and mixings. Briefly, starting with the precisely measured gauge couplings at scale  $M_Z$ , ISASUGRA evolves the three MSSM gauge couplings and third generation Yukawa couplings to a mass scale (determined to be  $\sim 2 \times 10^{16}$  GeV) where  $\alpha_1$  and  $\alpha_2$  unify. At this approximate unification scale,  $\alpha_3$  is set equal to  $\alpha_1$  and  $\alpha_2$ , and the GUT scale boundary condition values for  $m_0$ ,  $m_{1/2}$ ,  $A_0$  and  $B_0$  are implemented. From the approximate unification scale, the various soft SUSY breaking masses, gauge and Yukawa couplings are evolved via 26 RGE's to their weak scale values. We use 2-loop RGE's for gauge couplings, but only 1-loop RGE's for soft breaking terms. Weak scale sparticle threshold effects are included within the gauge coupling evolution. Soft breaking masses are evolved only down to the scale value equal to their mass value. At the electroweak scale, the 1-loop effective potential is minimized, allowing the replacement of  $B$  by  $\tan \beta$ , and evaluating the magnitude (but not the sign) of  $\mu$  in terms of  $M_Z$ . This procedure is iterated until a stable solution for all sparticle masses is obtained, consistent with grand unification and electroweak symmetry breaking.

After calculation of the spectra and couplings as detailed above, ISASUGRA then calculates all available sparticle decay modes and branching fractions. Currently, the program is valid only for  $\tan \beta \lesssim 10$ ; for very large values of  $\tan \beta$ , the effects from sbottom and stau mixing, not yet included, become important. It also assumes that the LSP is  $\tilde{Z}_1$ , which is not true for all choices of the parameters in set (1). Next, ISAJET generates all lowest order  $2 \rightarrow 2$  subprocesses for sparticle pair production according to their cross sections. The produced sparticles are then allowed to decay via the various possible cascades. Initial and final state parton showers are implemented, as well as hadronization and beam fragment evolution.

For detector simulation at the LHC, we use the toy calorimeter simulation package ISA-PLT. We simulate calorimetry covering  $-5 < \eta < 5$  with cell size  $\Delta\eta \times \Delta\phi = 0.05 \times 0.05$ . We take the hadronic energy resolution to be  $50\%/\sqrt{E} \oplus 0.03$  for  $|\eta| < 3$ , where  $\oplus$  denotes addition in quadrature, and to be  $100\%/\sqrt{E} \oplus 0.07$  for  $3 < |\eta| < 5$ , to model the effective  $p_T$  resolution of the forward calorimeter including the effects of shower spreading. We take electromagnetic resolution to be  $10\%/\sqrt{E} \oplus 0.01$ . Jets are found using fixed cones of size  $R = \sqrt{\Delta\eta^2 + \Delta\phi^2} = 0.7$  using the ISAJET routine GETJET. Clusters with  $E_T > 100$  GeV and  $|\eta(\text{jet})| < 3$  are labeled as jets. Muons and electrons are classified as isolated if they have  $p_T > 20$  GeV,  $|\eta(\ell)| < 2.5$ , and the visible activity within a cone of  $R = 0.3$  about the lepton direction is less than  $E_T(\text{cone}) = 5$  GeV.

## B. Signal versus background

To evaluate signals from supersymmetry in the multi-jet +  $E_T$  channel, we generate all possible supersymmetric subprocesses using ISAJET. Major physics backgrounds come from various SM processes which can give large amounts of missing transverse energy due to neutrinos produced in events, due to mis-measurement by calorimeter cells, and due to dead regions of the detector. We evaluate the following SM background processes:

- QCD multi-jet production (*e.g.*  $gg \rightarrow gg$  etc., where extra jet activity comes from parton showers, (this includes heavy flavor  $b\bar{b}$  and  $c\bar{c}$  production),

- $Z$ +multi-jet production, where  $Z \rightarrow \nu\bar{\nu}$  or  $\tau\bar{\tau}$ ,
- $W$ +multi-jet production, where  $W \rightarrow \ell\nu_\ell$  or  $\tau\nu_\tau$ ,
- $t\bar{t}$  production and decay.

We impose a series of cuts to extract signal from the vastly larger SM production cross sections. Since we wish to detect gluinos or squarks over a large mass range  $\sim 300\text{--}2000\text{ GeV}$ , different cuts are needed to optimize signal/background depending on the sparticle mass. After exploring a large variety of possible cuts for various SUGRA parameter choices, we arrived at the following requirements:

- no isolated leptons,
- transverse sphericity  $S_T > 0.2$  to reduce QCD dijet background,
- number of jets  $n(jets) \geq 2$  (jets as defined above),
- transverse plane angle  $\Delta\phi(\vec{H}_T, j_c)$  between  $\vec{H}_T$  and closest jet is  $30^\circ < \Delta\phi < 90^\circ$ .

After these mass-independent cuts, we apply a variable cut with the parameter  $E_T^c$  chosen depending on the gluino and squark masses:

- $\vec{H}_T > E_T^c$  and  $E_T(j_1), E_T(j_2) > E_T^c$ .

The results with these cuts for signal and total background levels are shown in Fig. 2, versus the cut parameter  $E_T^c$ . We show the signal cross sections for the six cases listed in Table I, which roughly correspond to  $m_{\tilde{g}} \sim 300, 800$  and  $1300\text{ GeV}$ , where  $m_{\tilde{q}} \sim m_{\tilde{g}}$  or  $m_{\tilde{q}} = (1.5 - 1.7)m_{\tilde{g}}$ . We also show the estimated background from the sum of all SM processes. Since the total SM cross section corresponds to about  $10^{15}$  events, it is obviously neither technically possible nor physically reasonable to generate realistic statistics for it. Instead, the various SM processes have been generated in several overlapping  $p_T$  ranges to obtain a reasonable estimate for all  $E_T^c$ . The background is discussed in more detail in Sec. IIc below.

From Fig. 2, we see that for  $E_T^c = 100\text{ GeV}$ , case 1 and 2 with  $m_{\tilde{g}} \sim 300\text{ GeV}$  are easily visible at levels of 5–10 above background, while the cases with heavier gluino masses are well below background. As the cut  $E_T^c$  is increased, the SM background decreases much more quickly than the heavy gluino signals. For  $E_T^c > 150\text{--}200\text{ GeV}$ , the cases with  $m_{\tilde{g}} \sim 800\text{ GeV}$  begin exceeding background. To see the signal from  $m_{\tilde{g}} \sim 1300\text{ GeV}$  above background, a hard cut of  $E_T^c > 300\text{--}400\text{ GeV}$  is needed. This agrees qualitatively with the results of Ref. [31], where two sets of cuts (soft and hard) were advocated to see light or heavy gluinos. As we will see shortly, gluino and squark mass values across the range of  $m_{\tilde{g}} \sim 300$  up to  $m_{\tilde{g}} \sim 1300\text{--}2000\text{ GeV}$  ought to be detectable. In particular, there should be no “undetectability window” in  $m_{\tilde{g}}$  between Fermilab Tevatron experiments of the Main Injector era, and LHC experiments

Fig. 2 also suggests a way to get a crude estimate of the gluino or squark mass. One plots the observed cross section versus  $E_T^c$  (for gradual stiffening of cuts), and compares with background expectations. The approximate range where  $m_{\tilde{g}}$  might lie can be obtained by measuring event rates for several values of  $E_T^c$ , starting at the point where observation begins

exceeding expectations from SM processes, and comparing against Monte Carlo expectation of the signal.

In Fig. 2, we have fixed  $A_0 = 0$  and  $\tan\beta = 2$ . Variations in  $A_0$  mainly affect third generation squark and slepton masses, so our results are relatively insensitive to different  $A_0$  values as long as the light stop  $\tilde{t}_1$  is not driven to too small a value. As an example, we plot in Fig. 3a the cross section after cuts (taking  $E_T^c = 300$  GeV) for  $m_0 = m_{1/2} = 300$  GeV (case 3) and also for  $m_0 = 2m_{1/2} = 600$  GeV, for five choices of  $A_0$ . Little variation is seen when  $A_0$  varies over the range shown. Multi-jet+ $\not{E}_T$  signals are also relatively insensitive to variations in  $\tan\beta$ . Case 3 is also plotted in Fig. 3b for five choices of  $\tan\beta$  and again shows only small differences in signal cross section.

### C. Reach of the LHC in SUGRA parameter space

Our next goal is to evaluate the reach of the LHC via the multi-jet+ $\not{E}_T$  signature in SUGRA parameter space. From Fig. 2, it is clear that for very heavy gluinos, a large value of  $E_T^c$  is desirable to enhance the signal relative to the background. For the heaviest gluinos and squarks observable at the LHC, which are roughly the heaviest consistent with SUSY relevant to electroweak symmetry breaking, we want to make a cut at about  $E_T^c = 500$  GeV. Only a very small fraction of the SM cross section passes such a cut, so it is necessary to combine events generated in several ranges of hard scattering  $p_T$  ( $p_T^{HS}$ ) for each SM process that can produce backgrounds. Table II lists the ranges generated for each process, the total number of events for each range, and the number of Monte Carlo events and the corresponding cross section passing the cut  $E_T^c = 500$  GeV. Fig. 4 shows the background cross sections for each process and range of  $p_T^{HS}$  vs.  $E_T^c$  for those values of  $E_T^c$  for which it is non-zero for the available statistics. While in retrospect a more uniform distribution of Monte Carlo events in  $\log p_T$  would have given a better estimate of the background, the samples listed in Table II are sufficient to provide an estimate of the SM background for all relevant values of  $E_T^c$ . In particular, for each  $E_T^c$  there are enough events in some range for each process to give an estimated background cross section greater than that from lower  $p_T$  ranges that produce no events. Therefore, we estimate the SM background as a function of  $E_T^c$  using the 95% upper limit calculated from the ranges giving a nonzero number of events, setting the background from the ranges giving zero events to zero. In particular, the total background from Table II then comes out to  $1.86 \pm 0.36$  fb, which gives a 95% CL upper bound on the total BG to be  $\sigma = 2.44$  fb. We conservatively use this value to obtain our  $5\sigma$  reach.

Since ISAJET generates higher order QCD processes using the branching approximation, it does not necessarily give the correct background for SUSY signatures, which typically involve “round” events with jets far from the collinear limit in which the branching approximation is correct. Fortunately, we find that our estimates of the SM background is smaller than the SUSY signal, so the SUSY mass reach is not very sensitive to the background estimate. Also, the significance of any signal is not dependent on the calculation of the SM backgrounds, since these can be determined from other data. Backgrounds from neutrinos from  $b$  and  $c$  decays can be checked against the  $p_T$  distribution of non-isolated muons. Backgrounds from  $Z \rightarrow \nu\bar{\nu}$  can be checked against measurements of  $Z \rightarrow \ell^+\ell^-$ . Backgrounds from  $W$  and  $t\bar{t}$  can be checked against distributions of isolated single and double leptons.

Detector induced backgrounds can be checked using jet-jet and  $\gamma$ -jet events. Given this data, it should be possible to determine the SM background, including the multijet and  $S_T$  cuts, accurately and so assign a significance limited only by statistics to any excess from SUSY.

The  $5\sigma$  background level calculated as described above is shown by the horizontal line in Fig. 5. (Notice that the signal to background ratio is very close to unity even for a signal just at this level so that we do not need to impose any other S/B requirement for the observability of the signal.) On the same plot, we show signal rates versus  $m_{\tilde{g}}$  for two cases: *i*) squares for  $m_0 = m_{1/2}$  ( $m_{\tilde{q}} \sim m_{\tilde{g}}$ ), and *ii*) triangles for  $m_0 = 4m_{1/2}$  ( $m_{\tilde{q}} \gg m_{\tilde{g}}$ ). From this plot, we see that for  $m_{\tilde{q}} \sim m_{\tilde{g}}$ , the LHC should be able to probe to  $m_{\tilde{g}} \sim 2000$  GeV, while for  $m_{\tilde{q}} > m_{\tilde{g}}$ , LHC should be able to probe to nearly  $m_{\tilde{g}} \sim 1300$  GeV. These results are in remarkably close agreement with the reach calculated in Ref. [31], which used somewhat different MSSM parameter choices and different cuts.

In Ref. [17], it was shown that in the minimal SUGRA model, the  $m_0$  *vs.*  $m_{1/2}$  plane forms a convenient panorama in which to plot various constraints. In Figs. 6–8, we plot the reach of the LHC in the multi-jet+ $\cancel{E}_T$  channel, using the  $5\sigma$  constraint for  $10 \text{ fb}^{-1}$  of collider data. For convenience, in frame *a*) we show contours in SUGRA parameter space; in frame *b*) we show corresponding gluino and squark (averaged over the 4 first generation squarks) mass contours. All the figures take  $A_0 = 0$  and  $m_t = 170$  GeV. Fig. 6 plots contours for  $\tan \beta = 2$  with  $\mu < 0$ , while Fig. 7 plots for the same value of  $\tan \beta$ , but with  $\mu > 0$ . Finally, Fig. 8 shows results for  $\tan \beta = 10$  and  $\mu < 0$ .

In these figures, the region shaded with bricks is excluded on theoretical grounds: either the correct electroweak symmetry breaking pattern is not obtained (or gives the wrong value of  $M_Z$ ), or the LSP is not the  $\tilde{Z}_1$ , but is instead the  $\tilde{W}_1$ , the  $\tilde{\tau}_1$ ,  $\tilde{\ell}_R$  or  $\tilde{\nu}_L$ . In addition, for some values of  $A_0$ , the light stop  $\tilde{t}_1$  can be driven tachyonic, so that electromagnetic and colour symmetries are spontaneously broken. The hatched regions are excluded by experiment. The experimentally excluded regions are formed [17] by combining bounds from LEP [3] that  $m_{\tilde{W}_1} > 47$  GeV,  $m_{H_\ell} > 60$  GeV, and  $m_{\tilde{\nu}} > 43$  GeV. In addition, the latest bound from CDF/D0 on multi-jets+ $\cancel{E}_T$  events [4] is included.

In Ref. [24], it was shown that LHC ought to be able to probe sleptons with mass  $m_{\tilde{l}} \sim 200\text{--}250$  GeV. The area to the left of the contour labelled  $\tilde{\ell}(200)$  denotes this region in SUGRA parameter space. Also, it was shown in Ref. [25] that (for  $\mu < 0$ ) LHC experiments ought to be able to explore much of the region below the contours labelled  $\tilde{Z}_2 \rightarrow \tilde{Z}_1 H_\ell$  and  $\tilde{Z}_2 \rightarrow \tilde{Z}_1 Z$  (above which the so-called spoiler modes become accessible), by searching for the clean trilepton signature of  $\tilde{W}_1 \tilde{Z}_2 \rightarrow 3\ell$ . This region also corresponds approximately to the maximal reach of Fermilab Tevatron collider experiments (although large holes of non-observability exist for some ranges of parameters due to a strong suppression of the  $\tilde{Z}_2 \rightarrow \tilde{Z}_1 \ell \ell$  branching fraction, especially for positive values of  $\mu$ ). Furthermore, LEP II should be able to explore the regions below the contours marked  $H_l(90)$  and  $\tilde{W}_1(90)$  where the lightest Higgs boson and the chargino are, respectively, lighter than 90 GeV.

In each of Figs. 6*a*–8*a*, we see the  $5\sigma$   $\cancel{E}_T$  reach is maximal for  $m_0 \sim \frac{1}{2}m_{1/2} \sim 500$  GeV, and drops to intercept the theoretically excluded (due to  $m_{\tilde{\tau}_1} < m_{\tilde{Z}_1}$ ) region around  $m_0 \sim 200$  GeV; this fall-off is due to the fact that as  $m_0$  decreases, sleptons become very light, resulting in the presence of many isolated leptons in the final state of gluino and squark cascade decays. The isolated lepton veto thus suppresses somewhat the multi-jet+ $\cancel{E}_T$  cross

section as  $m_0$  decreases; we may, however, expect that the multilepton cross section is large in this range of  $m_0$ . For not too large values of  $m_0$ , squark masses are somewhat lighter than (or comparable in mass to) gluinos, so that the combined cross section for  $\tilde{g}\tilde{g}$ ,  $\tilde{g}\tilde{q}$  and  $\tilde{q}\tilde{q}$  production is very large. In this region, the maximal reach of the LHC is obtained:  $m_{\tilde{g}} \sim 2000$  GeV can be explored. For  $m_0$  very large compared to  $m_{1/2}$ , squarks and sleptons are far heavier than gluinos. In this case, superparticle pair production is dominated by just  $\tilde{g}\tilde{g}$  production (for  $m_{\tilde{g}} < 1100$  GeV). Nevertheless, a mass reach of  $m_{\tilde{g}} \sim 1300$  GeV is obtained.

Recently, upper limits on sparticle masses have been obtained by requiring no fine-tuning in minimal SUGRA models [32]. These limits, which are somewhat subjective, suggest  $m_{\tilde{g}}, m_{\tilde{q}} \lesssim 700\text{--}800$  GeV. Comparison of these values with the calculated reach of the LHC suggests that LHC can perform a complete scan over the parameter space of minimal SUGRA models.

### III. CHARACTERISTICS OF THE MULTI-JET + $\cancel{E}_T$ SIGNAL

If supersymmetry is discovered, it will be important to see what information can be gleaned from signal events about the properties of super-particles. We have already mentioned that a rough determination of  $m_{\tilde{g}}$  and  $m_{\tilde{q}}$  can be made by noting the size of the signal cross section above background for different choices of the cut parameter  $E_T^c$ . In this section, we focus on several examples of intrinsic event properties, and the information they provide.

#### A. Jet multiplicity: Detecting squarks in the $\cancel{E}_T$ sample

If  $m_{\tilde{g}}$  is sufficiently smaller than  $m_{\tilde{q}}$ , then gluino pair production dominates, and each gluino decays typically via a lengthy cascade resulting in numerous final state jets, *e.g.*,  $\tilde{g} \rightarrow q\bar{q}\tilde{Z}_i$ ,  $\tilde{g} \rightarrow q\bar{q}\tilde{W}_i$  or  $\tilde{g} \rightarrow t\tilde{t}_1$ , followed by further  $\tilde{Z}_i$ ,  $\tilde{W}_i$ ,  $t$  and  $\tilde{t}_1$  decays. In contrast, if  $m_{\tilde{q}} \lesssim m_{\tilde{g}}$ , squarks decay through a more abbreviated cascade, via  $\tilde{q}_L \rightarrow q\tilde{W}_i$ ,  $q\tilde{Z}_i$ , and  $\tilde{q}_R \rightarrow q\tilde{Z}_i$  (Third generation squarks can, however, decay to charginos via their couplings to the Higgsino component). For right squarks,  $\tilde{q}_R \rightarrow q\tilde{Z}_1$  dominates over large regions of parameter space. Since hard jets are most likely to come from the primary decay, in multi-jet+ $\cancel{E}_T$  events, for a fixed value of  $m_{\tilde{g}}$ , one frequently expects a higher jet multiplicity if  $m_{\tilde{q}} > m_{\tilde{g}}$ , and  $\tilde{g}\tilde{g}$  production dominates, than if  $m_{\tilde{q}} < m_{\tilde{g}}$ , and  $\tilde{q}\tilde{q}$  and  $\tilde{q}\tilde{g}$  production dominates. (An alternative method involving the study of the charge asymmetry in the same sign dilepton sample was suggested in Ref. [28].)

This is explicitly illustrated in Fig. 9 where we plot the jet multiplicity after cuts (for the  $E_T^c$  value listed) for each of the SUGRA cases listed in Table 1. We have relaxed the jet cut to require only  $p_T(\text{jet}) > 50$  GeV for this plot, so that we increase the sensitivity to lower energy jets produced further down the cascade decay chain. The histograms shown include both signal and background contributions. In Fig. 9a, we show jet multiplicity for the two  $m_{\tilde{g}} \sim 300$  GeV cases (with  $E_T^c = 150$  GeV), where case 1 has  $m_{\tilde{q}} \sim m_{\tilde{g}}$ , and case 2 has  $m_{\tilde{q}} \gg m_{\tilde{g}}$ . We see that case 2 is dominated by 4 and 5 jet production, indicative of  $\tilde{g}\tilde{g}$  production and decay, whereas case 1 has a significantly lower average jet multiplicity,

and produces mainly 3 and 4 jet events more characteristic of a large component of  $\tilde{q}\tilde{q}$  production. In Fig. 9b, the two cases for  $m_{\tilde{g}} \sim 800$  GeV again show a larger jet multiplicity for the case where  $m_{\tilde{g}} \ll m_{\tilde{q}}$ . Finally, Fig. 9c shows the jet multiplicity for the two cases with  $m_{\tilde{g}} \sim 1400$  GeV, and again the  $m_{\tilde{g}} \ll m_{\tilde{q}}$  case has larger jet multiplicity. For case 6, we see that the jet multiplicity is large for  $n(\text{jet}) = 3$ , and then falls for  $n(\text{jet}) = 4$ , and rises again to a maximum for  $n(\text{jet}) = 5$ . This is due to a large background contribution in the  $n(\text{jet}) = 3$  bin.

In all cases, the  $n(\text{jet})$  distribution has a wide range of smearing. This is due to multiple hard partons produced at various stages along the cascade decay chain, but is also due to substantial initial and final state QCD radiation. Nonetheless, the final distributions do show that, if we have some idea of the gluino mass, the measured jet multiplicity can give a handle on whether or not the event sample contains a significant  $\tilde{q}$  production component, thus reflecting the relative values of  $m_{\tilde{g}}$  and  $m_{\tilde{q}}$ . Although we have illustrated this only for a few cases, we expect this to be a generic feature. The multiplicity in gluino events can only be reduced if the branching fraction for the radiative decay  $\tilde{g} \rightarrow g\tilde{Z}_1$  becomes very large.

We have also examined several other techniques for detecting the presence of squarks in the  $\cancel{E}_T$  sample. These are based on the expectation that heavy squark events (which form only a small fraction of the total sample) are expected to be more spherical and have larger jet multiplicities. For the first two cases in Table I, we have examined (i) the transverse sphericity distribution, (ii) the scatter plot of the transverse sphericity ( $S_T$ ) versus the “bigness”  $B = |\cancel{E}_T| + \sum |p_T(\text{jet})|$ , (iii) scatter plot of  $B$  versus  $k_T(\text{max})$ , the largest transverse momentum relative to the sphericity axis and (iv) the scatter plot of  $B$  versus  $n(\text{jet})$ . Only the last of these distributions appear to show any significant difference. Because this last distribution is correlated with the jet multiplicity distributions that we have already studied, we do not show it here.

## B. Gluino mass measurement

Although measurement of sparticle masses can proceed with significant precision at  $e^+e^-$  colliders [14] (given sufficient energy and luminosity), the situation is expected to be much more difficult in the environment of a hadron supercollider. This is especially true of measuring the mass of the gluino at the LHC. Even in the ideal case where all final state decay products of a gluino are tagged and precisely measured, the invariant mass distribution created will be a broad distribution between zero and  $m_{\tilde{g}} - m_{\tilde{Z}_1}$ . Real events will contain overlapping decay debris from both of the sparticles produced in the subprocess, in addition to significant amounts of QCD radiation, and imperfect detector effects.

In the past, various methods have been proposed for sparticle mass measurements at the LHC:

- In Ref. [33], associated production processes such as  $\tilde{g}\tilde{Z}_1$  were examined using parton level event generators. If these events could be singled out, then the ambiguities from producing and decaying *two* strongly interacting sparticles are by-passed. In practice, rather hard cuts were required to separate the  $\tilde{g}\tilde{Z}_1$  events from  $\tilde{g}\tilde{g}$  events. Ultimately, it was concluded that this reaction might be of use only if  $m_{\tilde{g}} \lesssim 350$  GeV.

- In Ref. [25], it was shown that  $m_{\tilde{Z}_2} - m_{\tilde{Z}_1}$  could be measured with significant precision from the end-point of the dilepton invariant mass distribution. However, the  $\tilde{W}_1\tilde{Z}_2 \rightarrow 3\ell$  signal upon which this is based is only observable in a limited region of parameter space.
- In Ref. [29], it was claimed that  $m_{\tilde{g}}$  could be measured to 15% by focussing on same-sign isolated dilepton events from  $\tilde{g}\tilde{g}$  production, where each gluino decays via  $\tilde{g} \rightarrow q\bar{q}\tilde{W}_1$ , with  $\tilde{W}_1 \rightarrow \ell\nu_\ell\tilde{Z}_1$ . However, these calculations may be overly optimistic, since this study considered only a single production mechanism ( $\tilde{g}\tilde{g}$  production—whereas same sign dileptons can come from various SUSY sources), a single cascade decay chain, and neglected effects of additional QCD radiation.

Here, we seek to measure the gluino mass in multi-jet+ $\cancel{E}_T$  events, following a similar path to Ref. [29]. We proceed as follows. First, we have a rough estimate of  $m_{\tilde{g}}$  and  $m_{\tilde{q}}$  by examining signal to background levels versus cut parameter  $E_T^c$ . After obtaining a relatively clean sample of signal events for an appropriate  $E_T^c$  value, we divide the event into two halves, using eigenvectors from constructing the transverse sphericity  $S_T$ . We then construct the invariant mass of jets in each of the two hemispheres, using only jets with  $p_T > E_T^c$ . Events are rejected if there is only one qualifying jet in each hemisphere. We then plot as  $M_{\text{est}}$  the maximal value of the mass of each hemisphere. Results are shown in Fig. 10 using  $m_0 = m_{1/2}$ ,  $A_0 = 0$ ,  $\tan\beta = 2$  and  $\mu < 0$ . The corresponding value of  $m_{\tilde{g}}$  is shown in each frame. Background level is shown by the shaded regions. In these plots, as usual, all supersymmetric subprocesses are contributing, with full cascade decays and QCD radiation effects, and detector smearing as given in Sec. IIa.

We see in Fig. 10a, using  $E_T^c = 100$  GeV for  $m_{\tilde{g}} \sim 300$  GeV, that the  $M_{\text{est}}$  distribution does indeed have a large smear due to the various effects listed previously. However, at least with our toy detector simulation, the two values of  $m_{\tilde{g}}$ , which differ by  $\sim 15\%$ , appear distinguishable. We plot values of  $M_{\text{est}}$  for  $m_{\tilde{g}} \sim 800$  GeV and  $E_T^c = 350$  GeV in Fig. 10b, and plot for  $m_{\tilde{g}} \sim 1500$  GeV with  $E_T^c = 600$  GeV in Fig. 10c. Again, values of  $m_{\tilde{g}}$  differing by  $\sim 15\%$  appear distinguishable. We note, however, that using a too small value of  $E_T^c$ , or too small a value of  $p_T(\text{jet})$ , can lead to a large amounts of smearing in these distributions, and loss of distinguishability. These distributions appear workable only for rather narrow ranges of cuts that guarantee sufficient hemispheric separation of event debris, and that only the hardest debris is used in constructing  $M_{\text{est}}$ , so that contamination of  $M_{\text{est}}$  is avoided. In Fig. 11, we show the same  $M_{\text{est}}$  plot, but now for  $m_0 = 4m_{1/2}$ , so that  $m_{\tilde{q}} \gg m_{\tilde{g}}$  (we show only the first two cases in Fig. 10 since the last case is not observable above background). The distributions appear somewhat less distinguishable than in Fig. 10, so that a mass resolution of 15% may be more difficult to attain in this case; nevertheless, distributions from gluino masses differing by 25% appear to be distinguishable. The jet multiplicity and/or  $B$ -multiplicity (see next section) may have to be used to distinguish whether  $m_{\tilde{q}} \gg m_{\tilde{g}}$  or  $m_{\tilde{q}} \sim m_{\tilde{g}}$ .

### C. Detecting Higgs bosons via $B$ -jets in cascade decay debris

Multi-jet+ $\cancel{E}_T$  events from gluino and squark cascade decays are expected to be unusually rich in heavy flavor content (mainly  $B$  mesons, and  $t$ -quarks, if kinematically allowed)

compared to SM processes [9,15,36]. This is due to a number of effects.

- The  $\tilde{t}_i$  and  $\tilde{b}_i$  masses are driven to values lower than the other squarks. This means decays like  $\tilde{g} \rightarrow t\tilde{t}_i$  or  $\tilde{g} \rightarrow b\tilde{b}_i$  can be kinematically allowed, and dominate decay rates for large enough values of  $m_{\tilde{g}}$ . Even if such decay modes are not allowed, three-body  $\tilde{g}$  decays to  $t\bar{t}\tilde{Z}_i$ ,  $t\bar{b}\tilde{W}_i$  and  $b\bar{b}\tilde{Z}_i$  are enhanced relative to decays to other squarks due to the larger propagator factor for the lighter top and bottom squarks.
- The various two- and three-body  $\tilde{g}$  decays to third generation quarks and squarks are further enhanced by the large third generation Yukawa couplings [34].
- $\tilde{Z}_i \rightarrow \tilde{Z}_j b\bar{b}$  decays are also enhanced by Higgs boson mediated decays [15].
- Higgs bosons can be produced in large quantities in  $\tilde{g}$  and  $\tilde{q}$  cascade decays. The various Higgs bosons frequently have dominant decays into 3rd generation particles, enhancing the heavy flavor content of  $\tilde{g}$  and  $\tilde{q}$  events [9].

In Table III, we list the average  $B$ -meson multiplicity in multi-jet+ $\cancel{E}_T$  events, for nine cases of SUGRA parameters. To construct our tabulation, we have required  $\cancel{E}_T > 200$  GeV,  $S_T > 0.2$ , and at least two jets with  $p_T(\text{jet}) > 100$  GeV and  $|\eta(\text{jet})| < 2.5$ . We then examine all jets with  $p_T > 50$  GeV in the same rapidity interval. If there is a  $B$ -hadron within  $\Delta R = 0.5$  of the jet, it is tagged as a  $B$  with 50% probability; otherwise, it is (mis)-tagged as a  $B$  with 2% probability [31]. From Table III, we see that in cases 1 and 2, for  $m_0 = 100$  GeV, the  $B$  multiplicity is rather low,  $\langle n_B \rangle \sim 0.9$ , compared with cases 3–9, with higher values of  $m_0$ . This is because *all* squarks and sleptons are relatively light, so any enhancements in production and/or decay to third generation quarks are small. For a fixed value of  $m_{\tilde{g}}$ , the highest  $B$  multiplicity occurs for the cases with large  $m_0$ , which are dominated by  $\tilde{g}\tilde{g}$  production, with enhanced cascade decays to heavy flavors: here,  $\langle n_B \rangle \sim 1.6$ . Cases 3–5, with intermediate values of  $m_0$ , also have intermediate values of  $\langle n_B \rangle \sim 1.1$ . We also see that, as discussed in Sec. IIIa, the average jet multiplicity is smaller for  $m_0$  small, and larger for  $m_0$  large.

Can one see direct evidence for Higgs production in cascade decay events? The light Higgs  $H_\ell$  is usually produced somewhere down the cascade decay chain via  $\tilde{Z}_2 \rightarrow \tilde{Z}_1 H_\ell$ . It has been shown in Ref. [35] that only in very limited regions of parameter space is the decay  $H_\ell \rightarrow \gamma\gamma$  likely to be visible. We have investigated cases 1–9 of Table II to see whether the  $H_\ell \rightarrow b\bar{b}$  decay can also be observed in cascade decay events. We do this by constructing the invariant mass  $m_{b\bar{b}}$  of all tagged  $B$ -jet pairs. Results are shown in Fig. 12. First we show case 1 in Fig. 12a, where  $m_0 = 100$  GeV, and  $\tilde{Z}_2$  dominantly decays to real sleptons and sneutrinos, so that Higgs production in SUSY events is minimal. In this case, a Higgs peak is not necessarily expected; we see a continuum distribution with only a slight bump at  $m_{H_\ell}$ . In Fig. 12b (case 3), where both gluino and squark pair production is important,  $\tilde{Z}_2 \rightarrow \tilde{Z}_1 H_\ell$  occurs at 94% branching ratio, the Higgs bump at  $m_{b\bar{b}} = 89$  GeV stands out against the continuum from other tagged  $B$ -jet pairs in the SUSY events. This is despite the fact that decays to  $b$  and  $t$  squarks constitute 60% of the gluino decays. Higgs production from the cascade decays of the first two generations of squarks remains observable. Finally, in Fig. 12c, we show the distribution for case 8, where  $\tilde{Z}_2 \rightarrow \tilde{Z}_1 H_\ell$  occurs with 98% branching ratio. However, in this case there are very many other sources of tagged  $B$ -jets from  $\tilde{g}$

cascade decays, especially  $\tilde{g} \rightarrow t\bar{t}\tilde{Z}_{1,2}$ ,  $b\bar{b}\tilde{Z}_{1,2}$  and  $\tilde{g} \rightarrow t\bar{b}\tilde{W}_i$ . Moreover, since  $\tilde{g}\tilde{g}$  production is by far the dominant process, there is a very high  $B$  multiplicity; then, the Higgs boson is frequently produced along with other  $B$ -jets, so that the combinatorial background tends to wash out the Higgs bump. The Higgs signal was also detectable at the appropriate Higgs mass in case 4; the signal did not stand out for the other four cases in Table III.

In conclusion, it appears that while the  $B$ -multiplicity is frequently enhanced above SM expectations, the  $H_\ell \rightarrow b\bar{b}$  signal can be identified only in limited regions of the parameter space: obviously, we need a substantial number of tagged  $B$ -jets from Higgs decay, but also that these events should not (as, for instance, in case 3) simultaneously contain other tagged  $B$ -jets which would then produce a large combinatorial background. Another requirement for the detection of the Higgs boson bump is that the rate from other sources of tagged  $B$ -jets (*e.g.*  $\tilde{g} \rightarrow \tilde{t}_1 t$  and  $b\bar{b}_1$  decays, where the squarks may be real or virtual) should not be overwhelmingly large.

#### IV. CONCLUSIONS

In this paper, we have performed a detailed analysis of the multi-jet+ $\cancel{E}_T$  signal expected from production and decay of supersymmetric particles within the framework of the minimal supergravity model, in which sparticle masses and couplings are fixed in terms of the parameter set (1). Assuming an integrated luminosity of  $10 \text{ fb}^{-1}$ , we have shown that the  $\cancel{E}_T$  signal (mainly from gluino and squark production and decay) should be observable in experiments at the LHC for gluino masses ranging from values accessible to Fermilab Tevatron experiments, up to nearly  $m_{\tilde{g}} \sim 1300 \text{ GeV}$  ( $m_{\tilde{g}} \sim 2000 \text{ GeV}$ ) for  $m_{\tilde{q}} \gg m_{\tilde{g}}$  (for  $m_{\tilde{q}} \sim m_{\tilde{g}}$ ), confirming earlier studies by the ATLAS collaboration [31]. We expect that the reach (in terms of sparticle masses) is not very sensitive to the details of the model as long as R-parity is conserved. Comparing the LHC reach in terms of  $m_{\tilde{g}}$  and  $m_{\tilde{q}}$  with somewhat subjective upper bounds from fine tuning constraints [32] (recall that the resolution of the fine-tuning problem provided the original motivation for phenomenological SUSY), it seems likely that LHC can perform a thorough search for  $R$ -conserving weak scale supersymmetry.

We show the SUSY reach via the multi-jets+ $\cancel{E}_T$  channel in the  $m_0$  *vs.*  $m_{1/2}$  plane of the minimal SUGRA model with gauge coupling unification and radiative electroweak symmetry breaking in Fig. 6–8. The relatively small parameter set yields a complete, highly correlated sparticle spectrum, so that the plot of the reach in the  $\cancel{E}_T$  channel can be compared with previous studies on the reach for sleptons and charginos/neutralinos. By comparing these various regions in Figs. 6–8, we see that of the channels studied, the reach in multi-jets+ $\cancel{E}_T$  is by far the largest. However, it should be kept in mind that multilepton signals (*e.g.* same-sign dileptons and trileptons) from cascade decays of gluinos and squarks may also probe some or all of this region. These signals would be especially important if  $m_0$  is very small, or if gluino decays to third generations fermions and sfermions are strongly enhanced. These multilepton signals could then provide a striking confirmation of a supersymmetric signal discovery in the multi-jet+ $\cancel{E}_T$  channel.

We have also studied what further information about sparticle properties can be obtained by a careful study of the  $\cancel{E}_T$  sample. We have used ISAJET to demonstrate that jet multiplicity can be a useful tool for detecting the presence of squarks in the  $\cancel{E}_T$  sample, and indirectly inferring the squark to gluino mass ratio. Of course, the distribution of jet

multiplicity is sensitive to the sparticle mass, so that this method is useful only after an estimate of the mass is obtained. We have further demonstrated that it might be possible to obtain a measure of the gluino mass by dividing each event in two halves, and using the greater of the masses in the two hemispheres as an estimator of  $m_{\tilde{g}}$ . We see from the distributions in Figs. 10 and 11 that gluino masses differing by 15–25% might be possible to distinguish. Since we have included the production of all sparticles in our simulation as well as contamination to the hemispheres from QCD jets, we believe that it would be worth testing this technique to see if it survives a detailed detector simulation. Finally, we have studied if signals from Higgs bosons produced by cascade decays of gluinos and squarks and decaying via  $H_\ell \rightarrow b\bar{b}$  are detectable. We conclude that, with reasonable  $B$  tagging efficiencies, this is possible but only for favourable ranges of parameters, where events containing Higgs bosons are relatively free of other  $B$ -jets, and further, that  $B$ -jets from other SUSY sources do not overwhelm the Higgs signal. It should nonetheless be kept in mind that SUSY events frequently tend to be rich in central  $B$ -jets, so that this may provide another handle for distinguishing SUSY from the SM, and gaining information on the squark to gluino mass ratio.

#### ACKNOWLEDGMENTS

This research was supported in part by the U. S. Department of Energy under contract number DE-FG05-87ER40319, DE-AC02-76CH00016, and DE-FG-03-94ER40833.

## REFERENCES

- [1] For a review of the minimal model and SUSY phenomenology, see H. P. Nilles, Phys. Rep. **110**, 1 (1984); H. Haber and G. Kane, Phys. Rep. **117**, 75 (1985); X. Tata, in *The Standard Model and Beyond*, p. 304, edited by J. E. Kim, World Scientific (1991); R. Arnowitt and P. Nath, *Lectures presented at the VII J. A. Swieca Summer School, Campos do Jordao, Brazil, 1993 CTP-TAMU-52/93*; V. Barger and R. J. N. Phillips, Wisconsin preprint, MAD/PH/765 (1993); *Properties of SUSY Particles*, L. Cifarelli and V. Khoze, Editors, World Scientific (1993).
- [2] U. Amaldi, W. de Boer and H. Fürstenau, Phys. Lett. **B260**, 447 (1991); J. Ellis, S. Kelley and D. Nanopoulos, Phys. Lett. **B260**, 131 (1991); P. Langacker and M. Luo, Phys. Rev. **D44**, 817 (1991).
- [3] D. Decamp *et.al.* (ALEPH Collaboration), Phys. Rep. **216**, 253 (1992) and Phys. Lett. **B244**, 541 (1990). P. Abreu *et.al.* (DELPHI Collaboration), Phys. Lett. **B247**, 157 (1990); O. Adriani *et.al.* (L3 Collaboration), Phys. Rep. **236**, 1 (1993); M. Akrawy *et.al.* (OPAL Collaboration), Phys. Lett **B240**, 261 (1990) and Phys. Lett. **B248**, 211 (1990). For a review, see G. Giacomelli and P. Giacomelli, Riv. Nuovo Cim. **16**, 1 (1993).
- [4] M. Paterno, Ph.D. thesis; D. Claes (D0 Collaboration), *presented at the 8th DPF meeting, Albuquerque, NM, Aug. 1994*; F. Abe *et. al.* (CDF Collaboration), Phys. Rev. Lett. **69**, 3439 (1992).
- [5] H. Baer and X. Tata, Phys. Rev. **D47**, 2739 (1993); H. Baer, C. Kao and X. Tata, Phys. Rev. **D48**, 5175 (1993); H. Baer, C-H. Chen, C. Kao and X. Tata, paper in preparation.
- [6] T. Kamon, J. Lopez, P. McIntyre and J. T. White, Phys. Rev. **D50**, 5676 (1994).
- [7] H. Baer *et. al.*, to appear in *Electroweak Symmetry Breaking and Beyond the Standard Model*, edited by T. Barklow, S. Dawson, H . Haber and J. Seigrist, (World Scientific) 1995.
- [8] JLC-1, KEK Report 92-16 (1992).
- [9] H. Baer, X. Tata and J. Woodside, Phys. Rev. **D45**, 142 (1992); H. Baer, M. Bisset, X. Tata and J. Woodside, Phys. Rev. **D46**, 303 (1992); C. Albajar *et. al.* in Aachen LHC Collider Workshop, CERN90-10 (1990); F. Pauss, *ibid*; H. Baer *et. al.* in *Research Directions for the Decade*, E. Berger, Editor (World Scientific, 1992).
- [10] The Solenoidal Detector Collaboration Technical Design Report, SDC92-201 (1992).
- [11] GEM Collaboration, Technical Design Report, GEM-TN-93-262 (1993).
- [12] F. Paige and S. Protopopescu, in *Supercollider Physics*, p. 41, ed. D. Soper (World Scientific, 1986); H. Baer, F. Paige, S. Protopopescu and X. Tata, in *Proceedings of the Workshop on Physics at Current Accelerators and Supercolliders*, ed. J. Hewett, A. White and D. Zeppenfeld, (Argonne National Laboratory, 1993).
- [13] We will refer to these models as SUGRA models and distinguish these analyses from the MSSM model analyses discussed above. We, however, warn the reader that MSSM has also been used by some authors to refer to the minimal SUGRA model. We feel that it is appropriate to keep in mind the distinctions between the two models which are based on somewhat different assumptions: SUGRA models incorporate specific (well-motivated) assumptions, spelled out later in the text, about physics at high energy scales, and are more restrictive. Yet more constrained models (based on superstring theories) depend on just two parameters as discussed *e.g.* by A. Brignole, L. Ibañez and C. Muñoz, Nucl. Phys. **B422**, 125 (1994).

- [14] T. Tsukamoto, K. Fujii, H. Murayama, M. Yamaguchi and Y. Okada, KEK preprint 93-146 (1993), to appear in Phys. Rev. **D**.
- [15] H. Baer, M. Drees, C. Kao, M. Nojiri and X. Tata, Phys. Rev. **D50**, 2148 (1994).
- [16] J. Lopez, D. Nanopoulos, G. Park, X. Wang and A. Zichichi, Phys. Rev. **D50**, 2164 (1994).
- [17] H. Baer, C-H. Chen, R. Munroe, F. Paige and X. Tata, Phys. Rev. **D51**, 1046 (1995).
- [18] See *e.g.* L. Hall, J. Lykken and S. Weinberg, Phys. Rev. **D27**, 2359 (1983) and references therein.
- [19] L. Ibañez, Phys. Lett. **B303**, 55 (1993).
- [20] K. Inoue, A. Kakuto, H. Komatsu and H. Takeshita, Prog. Theor. Phys. **68**, 927 (1982) and **71**, 413 (1984).
- [21] Some recent analyses of supergravity mass patterns include, G. Ross and R. G. Roberts, Nucl. Phys. **B377**, 571 (1992); R. Arnowitt and P. Nath, Phys. Rev. Lett. **69**, 725 (1992); M. Drees and M. M. Nojiri, Nucl. Phys. **B369**, 54 (1993); S. Kelley, J. Lopez, D. Nanopoulos, H. Pois and K. Yuan, Nucl. Phys. **B398**, 3 (1993); M. Olechowski and S. Pokorski, Nucl. Phys. **B404**, 590 (1993); V. Barger, M. Berger and P. Ohmann, *ibid.* **49**, 4908 (1994); G. Kane, C. Kolda, L. Roszkowski and J. Wells, Phys. Rev. **D49**, 6173 (1994); D. J. Castaño, E. Piard and P. Ramond, Phys. Rev. **D49**, 4882 (1994); W. de Boer, R. Ehret and D. Kazakov, Karlsruhe preprint, IEKP-KA/94-05 (1994); H. Baer, C.H. Chen, R. Munroe, F. Paige and X. Tata, Ref. [17].
- [22] B. Campbell, Phys. Rev. **D28**, 209 (1983); F. Gabbiani and A. Masiero, Nucl. Phys. **B322**, 235 (1989).
- [23] L. Ibañez and G. Ross, Phys. Lett. **B110**, 215 (1982); L. Ibañez, Phys. Lett. **B118**, 73 (1982); J. Ellis, D. Nanopoulos and K. Tamvakis, Phys. Lett. **B121**, 123 (1983); L. Alvarez-Gaumé, J. Polchinski and M. Wise, Nucl. Phys. **B121**, 495 (1983).
- [24] F. del Aguila and Ll. Ametller, Phys. Lett. **B261**, 326 (1991); H. Baer, C-H. Chen, F. Paige and X. Tata, Phys. Rev. **D49**, 3283 (1994)
- [25] H. Baer, C-H. Chen, F. Paige and X. Tata, Phys. Rev. **D50**, 4508 (1994).
- [26] J. Botts *et. al* Phys. Lett. **B304**, 159 (1993).
- [27] H. Baer *et. al.*, Phys. Lett. **B161**, 175 (1985); G. Gamberini. Z. Phys. **C30**, 605 (1986); H. Baer, V. Barger, D. Karatas and X. Tata, Phys. Rev. **D36**, 96 (1987); G. Gamberini, G. Giudice, B. Mele and G. Ridolfi, Phys. Lett. **203B**, 453 (1988); R. M. Barnett, J. Gunion and H. Haber, Phys. Rev. **D37**, 1892 (1988); A. Bartl, W. Majerotto, B. Mosslacher and N. Oshimo, Z. Phys. **C52**, 477 (1991).
- [28] H. Baer, X. Tata and J. Woodside, Ref. [9].
- [29] R. M. Barnett, J. Gunion and H. Haber, Phys. Lett. **B315**, 349 (1993).
- [30] See also K. Lane, F. Paige, T. Skwarnicki and W. Womersley, Brookhaven preprint, BNL-61138 (1994).
- [31] ATLAS Collaboration, Letter of Intent, CERN/LHCC/92-4 (1992). The values of the reach are consistent with the updated numbers in the ATLAS Technical proposal, CERN/LHCC 94-3.
- [32] R. Barbieri and G. Giudice, Nucl. Phys. **B306**, 63 (1988); see G. Anderson and D. Castano, MIT-CTP-2369 (1994), for an updated measure of fine-tuning, and associated limits on sparticle masses.
- [33] H. Baer, D. Karatas and X. Tata, Phys. Rev. **D42**, 2259 (1990).

- [34] H. Baer, X. Tata and J. Woodside, Phys. Rev. **D42**, 1568 (1990); A. Bartl, W. Majerotto, B. Mosslacher, N. Oshimo and S. Stippel, Phys. Rev. **D43**, 2214 (1991).
- [35] See H. Baer, M. Bisset, X. Tata and J. Woodside, Ref. [9].
- [36] A. Bartl, W. Majerotto and W. Porod, Z. Phys. **C64**, 499 (1994).

## TABLES

TABLE I. Six parameter choices used for cross section evaluation of multi-jet +  $\cancel{E}_T$  events. We take  $A_0 = 0$ ,  $\tan \beta = 2$  and  $\text{sgn}(\mu) < 0$ . Also,  $m_t = 170$  GeV.

Case	$m_0$	$m_{1/2}$	$m_{\tilde{g}}$	$m_{\tilde{q}}$
1	100	100	290	270
2	400	100	310	460
3	300	300	770	720
4	1200	300	830	1350
5	600	600	1400	1300
6	2000	500	1300	2200

TABLE II. Details of background calculation after cuts using cut parameter  $E_T^c = 500$  GeV. We list the background process ( $BG$ ), the range of hard scattering  $p_T$  ( $p_T^{HS}$ ) over which they were evaluated, the number of events generated ( $N$ ), number of events passing cuts ( $N_{cut}$ ), total BG cross section ( $\sigma_{tot}$  in fb), and background cross section after cuts ( $\sigma_{cut}$  in fb). We compute the combined background to be  $\sigma = 1.86 \pm 0.36$  fb, which yields a 95% CL upper limit of  $\sigma = 2.44$  fb, which we use for the computation of the LHC reach. We take  $m_t = 170$  GeV.

$BG$	$p_T^{HS}$	$N$	$N_{cut}$	$\sigma_{tot}$	$\sigma_{cut}$
$QCD$	200-1000	$2.843 \times 10^7$	0	$8.9 \times 10^7$ fb	—
$QCD$	500-1000	$10^5$	0	1085	—
$QCD$	800-2000	$2 \times 10^6$	17	$8.0 \times 10^5$	$(6.8 \pm 1.6) \times 10^{-1}$
$QCD$	2000-3000	$2.5 \times 10^5$	21	103	$(8.7 \pm 1.9) \times 10^{-3}$
$t\bar{t}$	500-1000	$5.5 \times 10^5$	0	$7.2 \times 10^5$	—
$t\bar{t}$	1000-2000	$1 \times 10^5$	14	0.48	$(6.7 \pm 1.8) \times 10^{-3}$
$W+\text{jets}$	10-800	$1.78 \times 10^7$	0	$3.1 \times 10^7$	—
$W+\text{jets}$	300-800	$4 \times 10^5$	9	$9.9 \times 10^3$	$(2.2 \pm 0.74) \times 10^{-1}$
$W+\text{jets}$	800-2000	$8 \times 10^5$	1105	0.89	$(1.2 \pm 0.04) \times 10^{-1}$
$Z+\text{jets}$	100-300	$5 \times 10^4$	0	147	—
$Z+\text{jets}$	300-1000	$2.5 \times 10^4$	6	$3 \times 10^3$	$(7.3 \pm 3.0) \times 10^{-1}$
$Z+\text{jets}$	1000-2000	$1 \times 10^5$	1314	7.0	$(9.1 \pm 0.25) \times 10^{-2}$

TABLE III. Nine cases examined for  $B$ -multiplicity, and the possibility of reconstructing a Higgs mass via  $m(b\bar{b})$ . We take  $A_0 = 0$ , and  $\mu < 0$ , except for case 4, for which  $\mu > 0$ . All mass quantities are in units of GeV.

Case	$m_0$	$m_{1/2}$	$\tan \beta$	$m_{H_\ell}$	$\langle n(b\text{-tag}) \rangle$	$\langle p_T(b\text{-tag}) \rangle$	$\langle n(\text{no-tag}) \rangle$	$\langle p_T(\text{no-tag}) \rangle$
1	100	300	2	87.7	0.90	127	4.5	124
2	100	300	10	116.6	0.90	126	4.5	124
3	300	300	2	88.4	1.16	121	4.6	121
4	300	300	2	102.5	1.18	124	4.7	121
5	300	300	10	116.6	1.04	123	4.7	121
6	600	300	2	90.0	1.65	118	5.1	113
7	600	300	10	117.2	1.31	124	5.7	119
8	1000	275	2	92.3	1.59	126	5.8	123
9	1000	350	10	120.5	1.68	128	6.2	122

## FIGURES

FIG. 1. Total cross section for strongly interacting sparticle pairs (solid), associated production of gluinos or squarks with charginos or neutralinos (dot-dashed) and chargino/neutralino production (dashes), for *a*)  $m_{\tilde{q}} = m_{\tilde{g}}$  and *b*)  $m_{\tilde{q}} = 2m_{\tilde{g}}$ , as a function of  $m_{\tilde{g}}$ , for  $pp$  collisions at  $\sqrt{s} = 14$  TeV.

FIG. 2. Cross section in fb after cuts, as a function of cut parameter  $E_T^c$ , for total background ( $\times$ 's), and for the six signal cases listed in Table 1.

FIG. 3. *a*) Cross section in fb after cuts, as a function of  $A_0/m_0$ , for parameter choices shown. In *b*), we show variation in the cross section for Table 3 case 3 when  $\tan \beta$  is varied.

FIG. 4. Background cross sections vs.  $E_T^c$  obtained from various samples of events. The  $p_T^{HS}$  range of the hard scattering subprocesses is listed.

FIG. 5. Signal cross sections for  $m_0 = m_{1/2}$  (squares) and  $m_0 = 4m_{1/2}$  (triangles), after cuts, using  $E_T^c = 500$  GeV, as a function of  $m_{\tilde{g}}$ . We also show the  $5\sigma$  background cross section assuming an integrated luminosity of  $10 \text{ fb}^{-1}$ . We take  $A_0 = 0$ ,  $\tan \beta = 2$ , and  $\mu < 0$ .

FIG. 6. In *a*), we show regions of SUGRA parameter space excluded by theory (bricks), excluded by experiments (slashed), and regions explorable by LHC assuming integrated luminosity of  $10 \text{ fb}^{-1}$ , for  $A_0 = 0$ ,  $\tan \beta = 2$ , and  $\mu < 0$ . We also show regions explorable via slepton searches at LHC, and Higgs and chargino searches at LEP II. Much of the region below the spoiler mode ( $\tilde{Z}_2 \rightarrow \tilde{Z}_1 Z$  and  $\tilde{Z}_2 \rightarrow \tilde{Z}_1 H_l$ ) contour is explorable via isolated trileptons at both Tevatron and LHC. In *b*), we show the same plane, but with various mass contours for  $m_{\tilde{g}}$  and  $m_{\tilde{q}}$  (averaged over 1st generation).

FIG. 7. Same as Figure 5, except for  $\mu > 0$ .

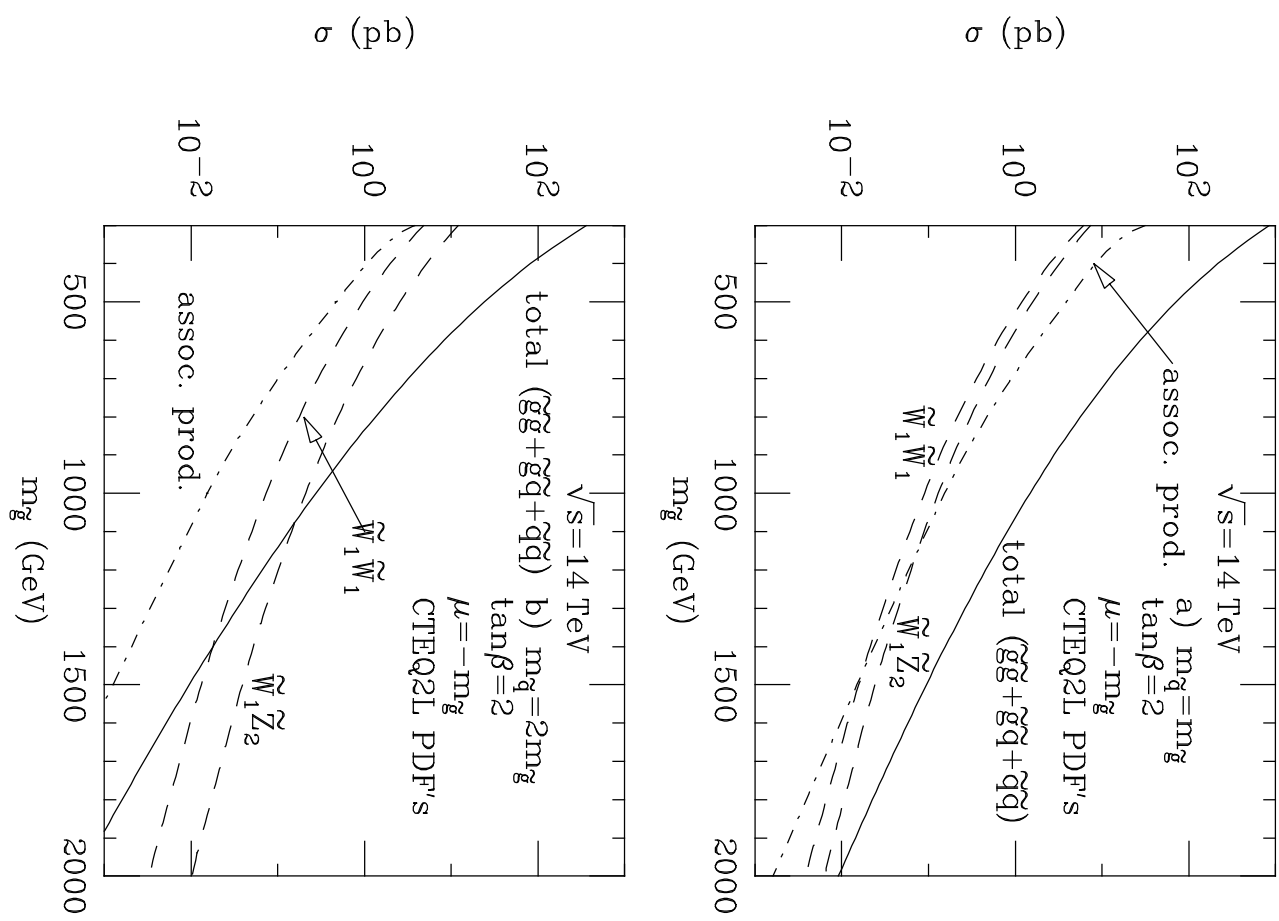
FIG. 8. Same as Figure 5, except for  $\tan \beta = 10$ .

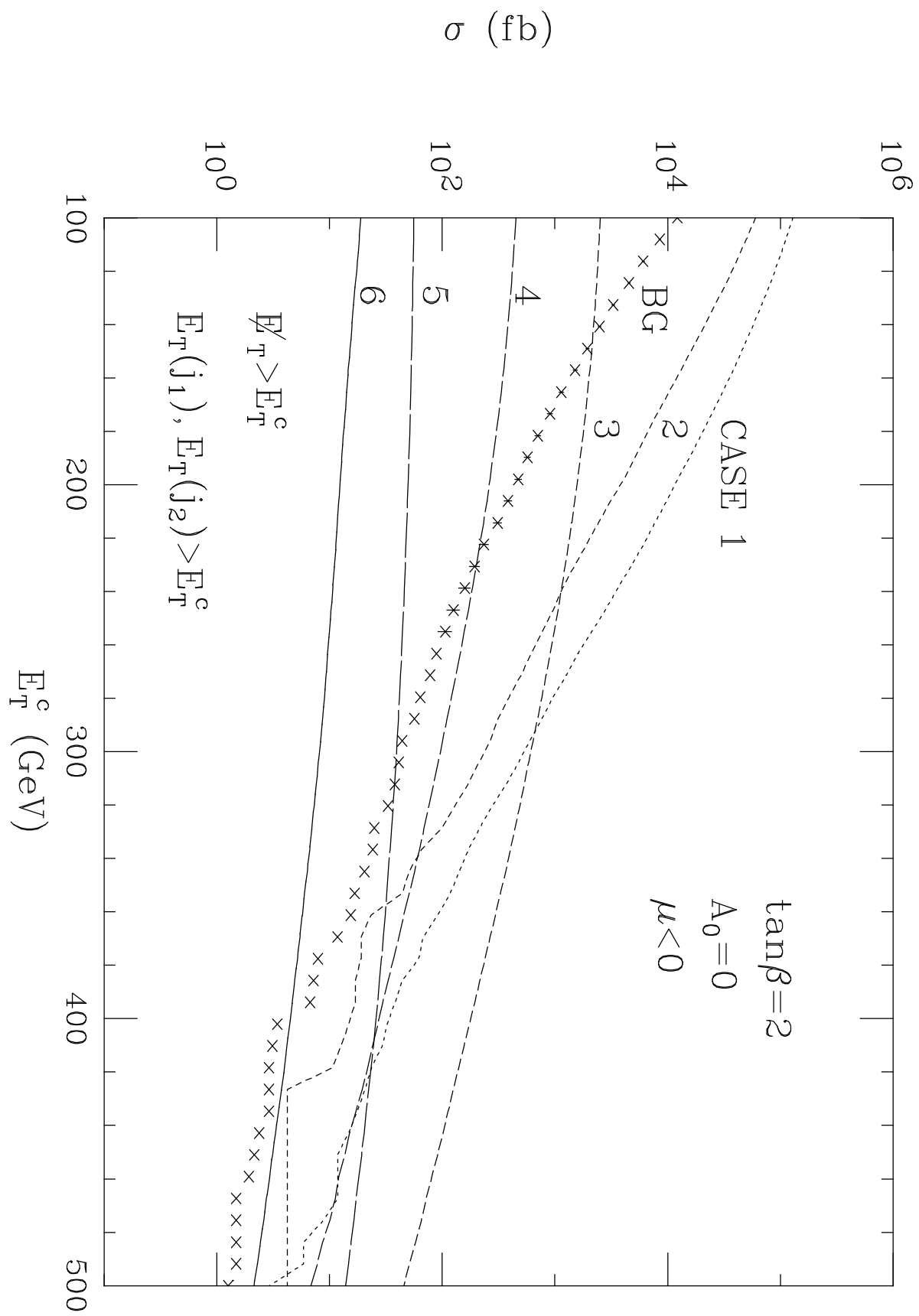
FIG. 9. Fractional jet multiplicity after cuts (signal plus background), for six cases listed in Table 1, for different values of  $E_T^c$ . The jet  $p_T$  cut has been relaxed to  $p_T(\text{jet}) > 50$  GeV.

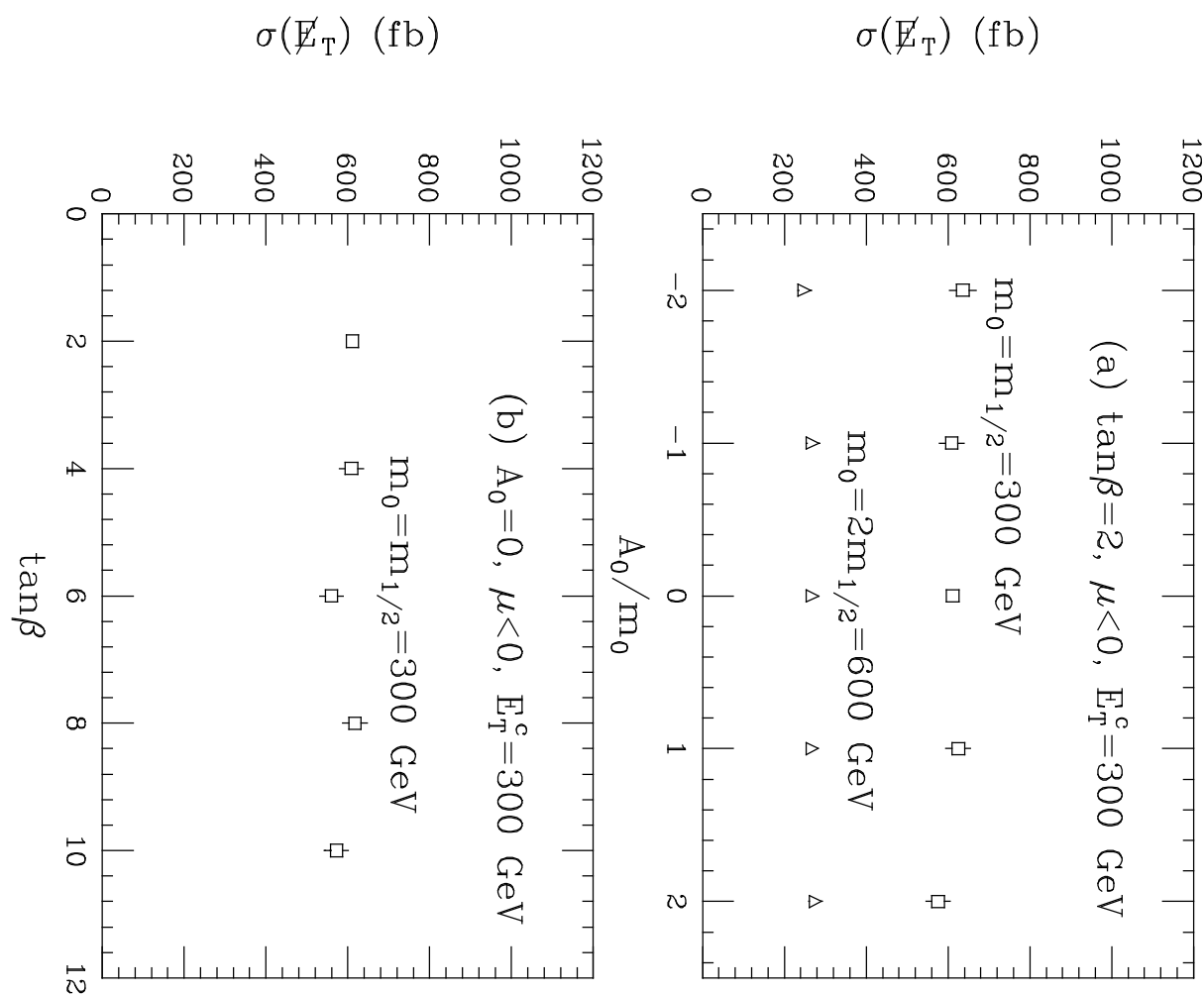
FIG. 10. Distribution in  $M_{est}$  for different values of  $m_{\tilde{g}}$  and cut parameter  $E_T^c$ , along with background contribution (shaded).  $M_{est}$  is formed after cuts by dividing the event into hemispheres via the transverse sphericity eigenvector, forming the invariant mass of the jets, and taking the maximal value. Events with only one jet in a hemisphere are rejected. We take  $m_0 = m_{1/2}$ .

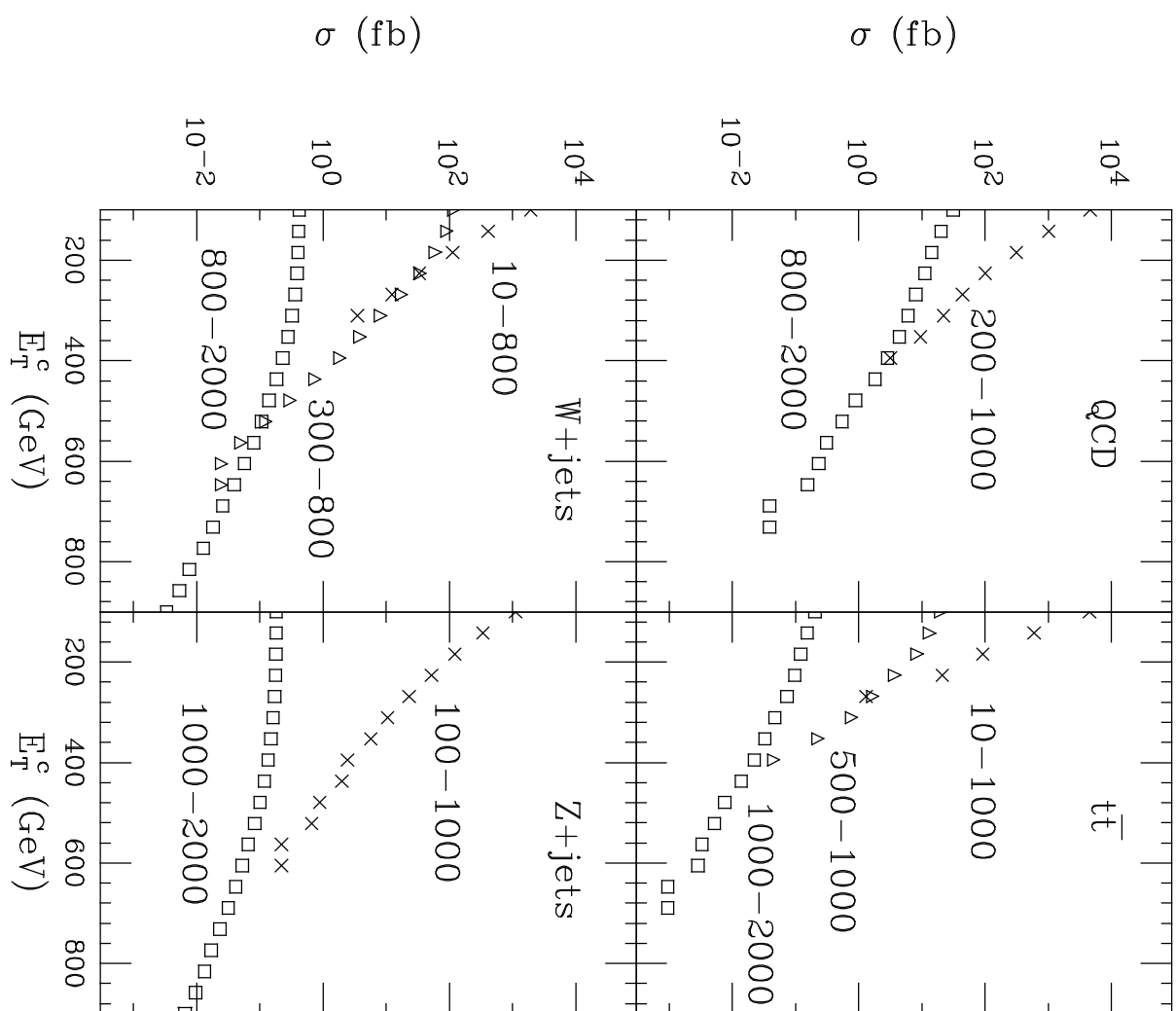
FIG. 11. Same as Fig. 10, except we take  $m_0 = 4m_{1/2}$ .

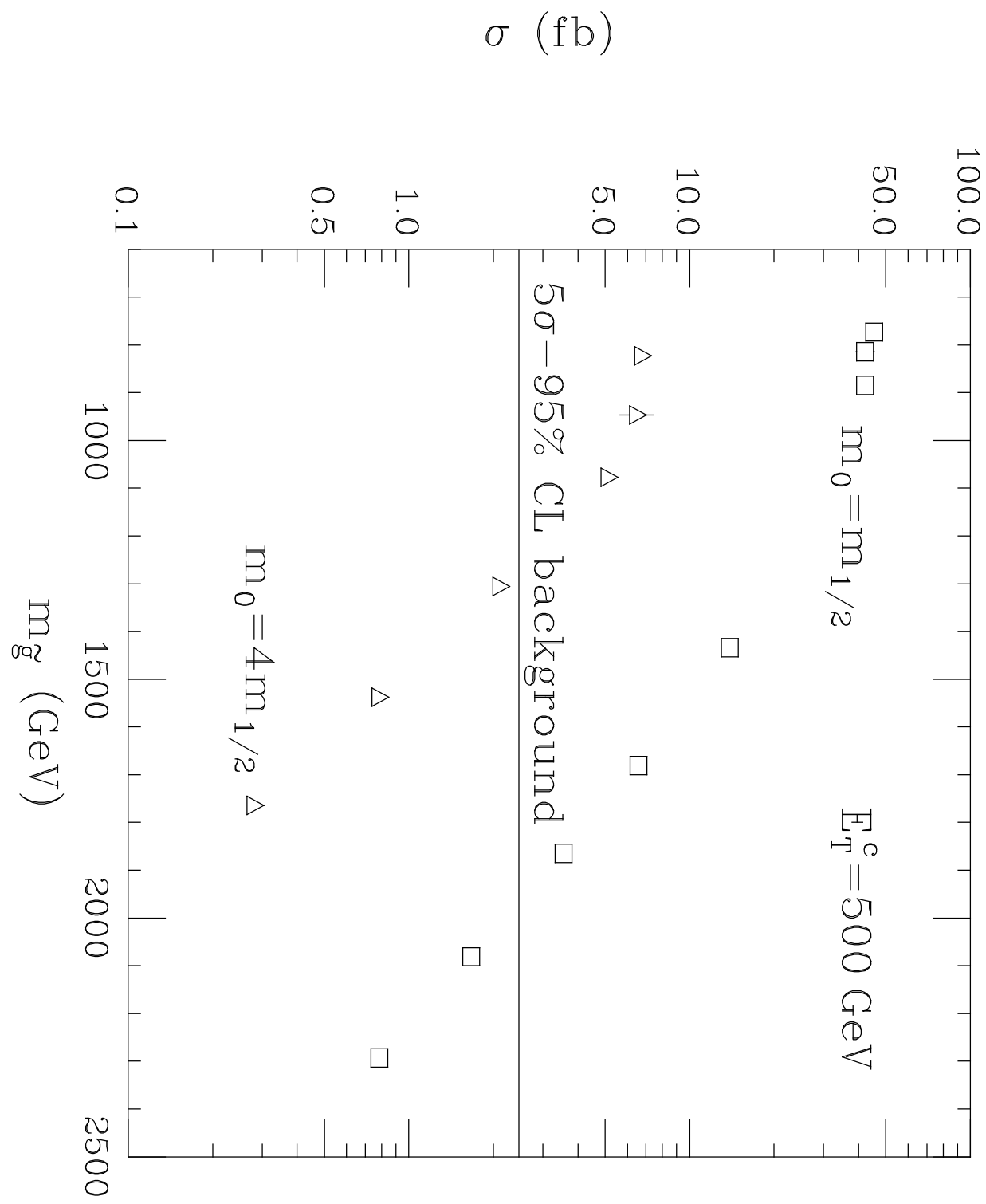
FIG. 12. Mass distributions for pairs of tagged  $b$  jets. (a) Case 1 from Table III. Higgs production is small. (b) Case 3 from Table III.  $B(\tilde{Z}_2 \rightarrow \tilde{Z}_1 H_\ell) = 94\%$ , and peak is observed at  $m_{H_\ell}$ . (c) Case 8 from Table III.  $B(\tilde{Z}_2 \rightarrow \tilde{Z}_1 H_\ell) = 98\%$ , but more combinatorial background.

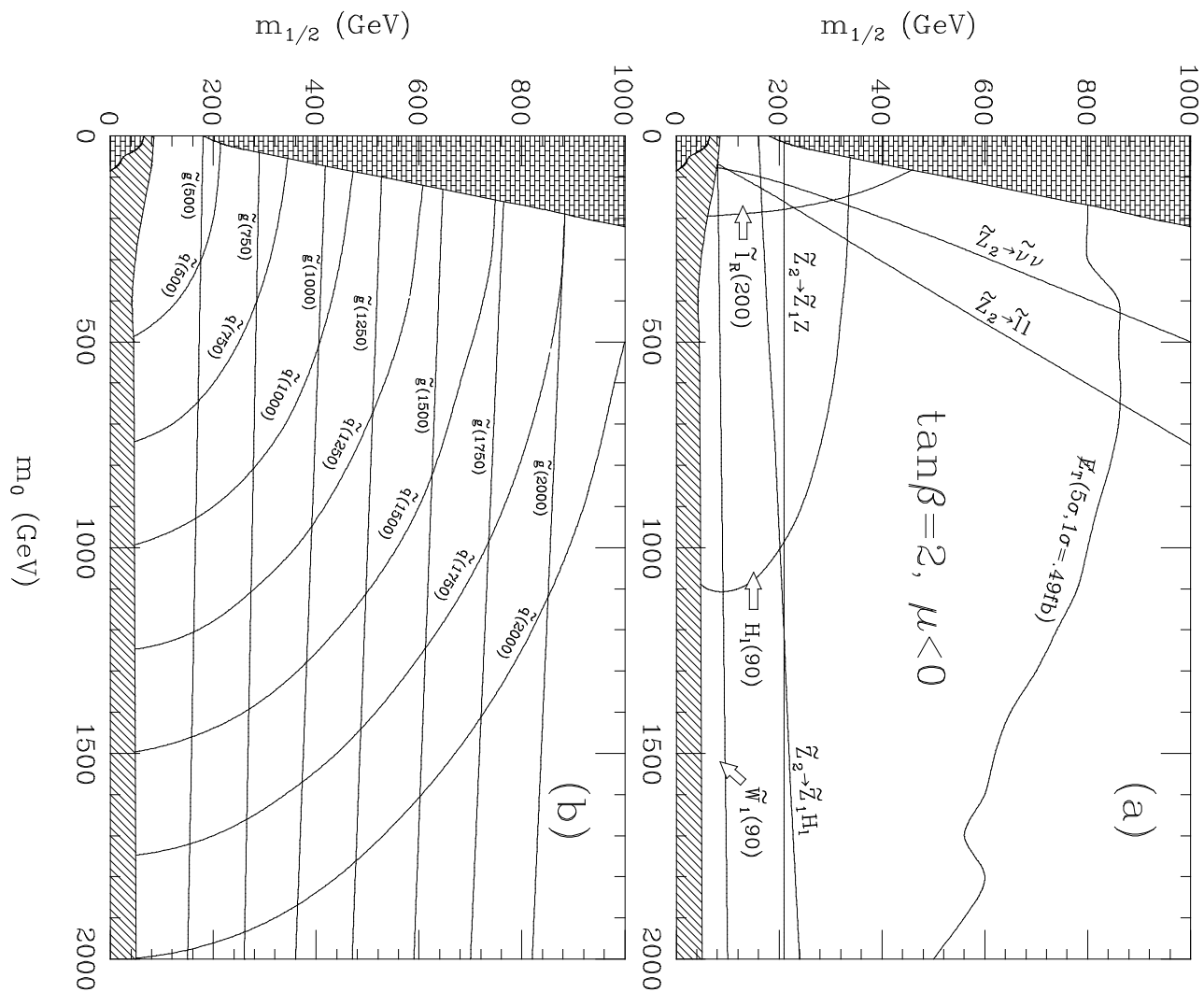


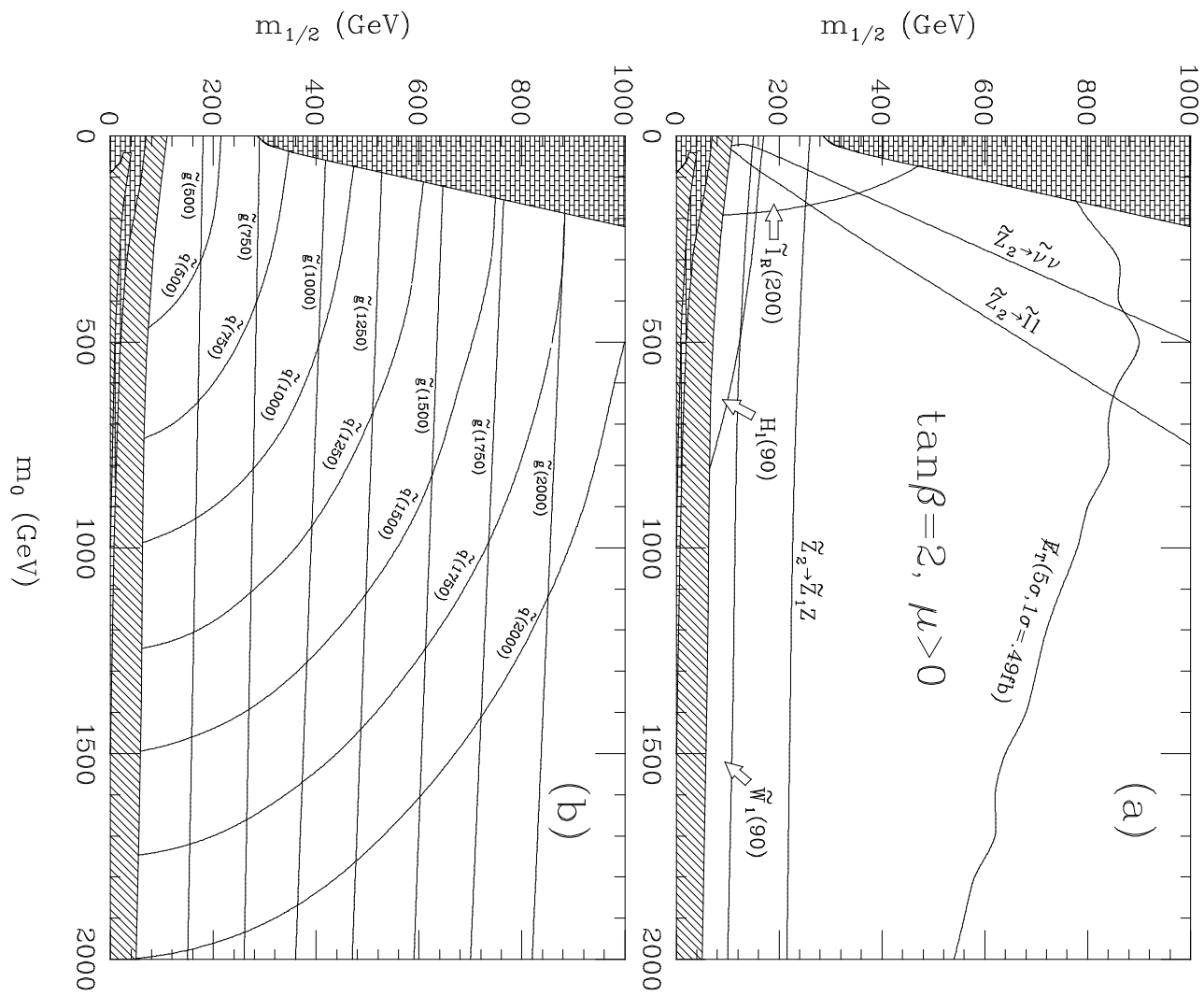


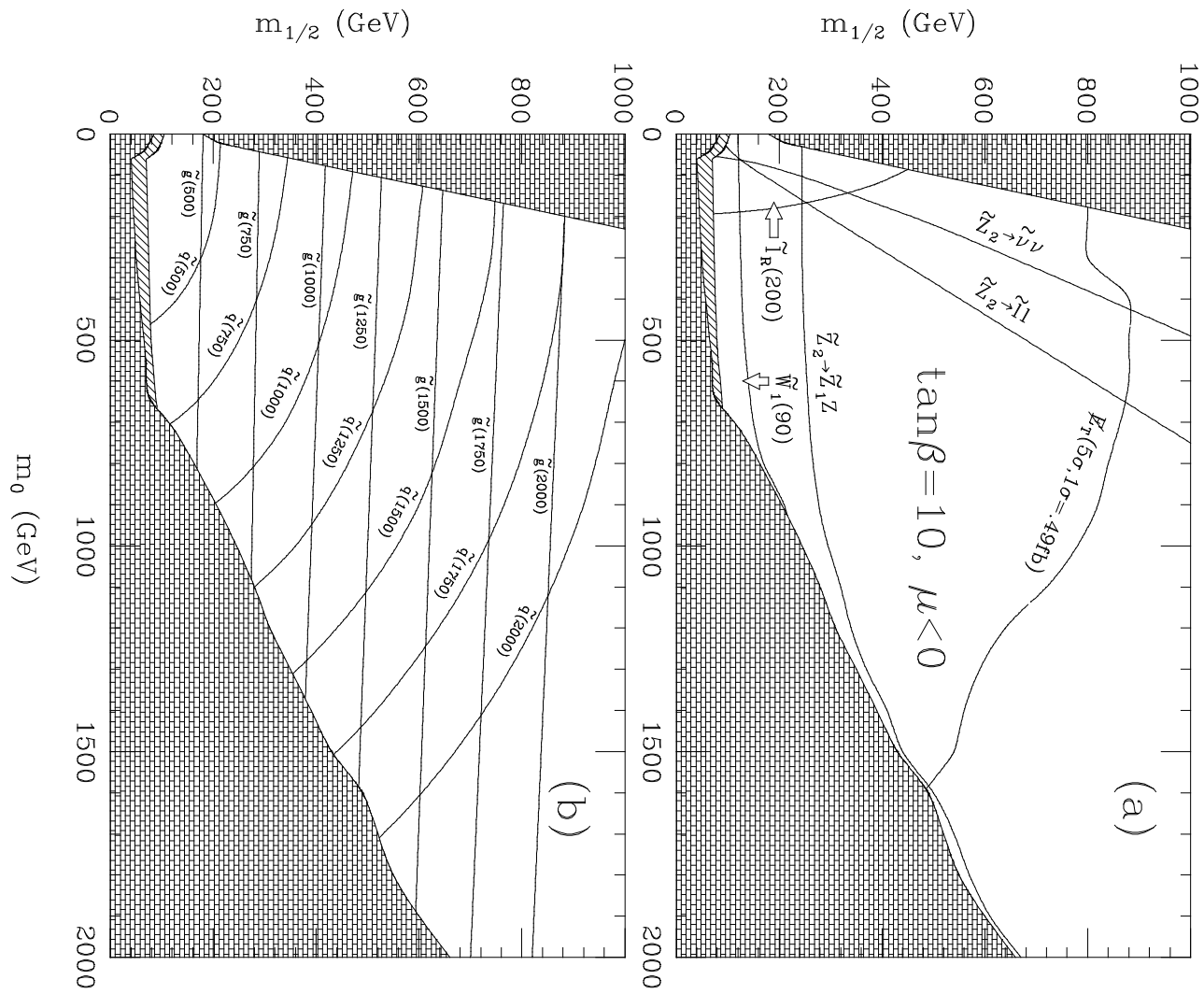












### Fractional jet multiplicity

